Improving the thermoelectric performance of p-type $(Bi_xSb_{1-x})_2Te_3$ thin films via tuning Bi_xSb_{1-x} layer

Hang Ju[1,a‡], Beibei Zhu[1,a,*‡], Wenya Wang[a], Lili Chen[a], Xianfeng Ni[b,*], Li Tao[a,*]

a School of Materials Science and Engineering, Jiangsu Key Laboratory of Advanced Metallic Materials, Southeast University, Nanjing 211189, People's Republic of China. E-mail: tao@seu.edu.cn, 101012333@seu.edu.cn

b Institute for Next Generation Semiconductor Materials, Southeast University, Suzhou 215123, People's Republic of China. E-mail: 103200036@seu.edu.cn

‡ H.J. and B.Z. contributed equally to this work

Table S1 The abbreviation of the investigated samples

Sample abbreviation	Thin film	Synthesis process
as-grown-BS	Bi_xSb_{1-x}	Electron beam evaporation (EBE)
an-100-BS	Bi_xSb_{1-x}	EBE+annealing under 100°C
an-150-BS	Bi_xSb_{1-x}	EBE+annealing under 150°C
an-200-BS	Bi_xSb_{1-x}	EBE+annealing under 200°C
as-grown-BST	$(Bi_xSb_{1-x})_2Te_3$	EBE+thermally-assisted conversion (TAC)
an-100-BST	$(Bi_xSb_{1-x})_2Te_3$	EBE+annealing under 100°C+TAC
an-150-BST	$(Bi_xSb_{1-x})_2Te_3$	EBE+annealing under 150°C+TAC
an-200-BST	$(Bi_xSb_{1-x})_2Te_3$	EBE+annealing under 200°C+TAC

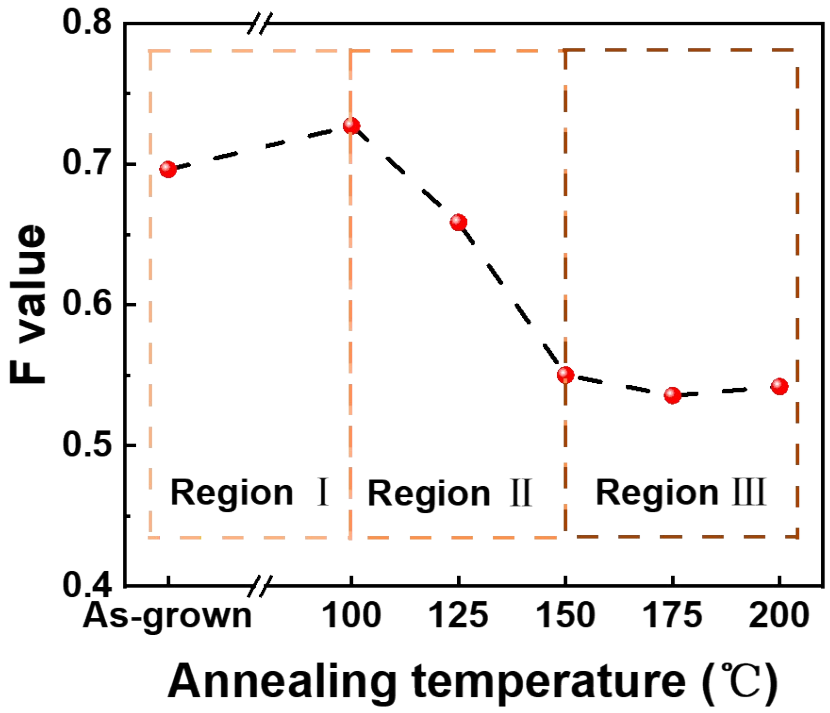

Figure S1 F values of the $(Bi_xSb_{1-x})_2Te_3$ thin films under different annealing temperatures

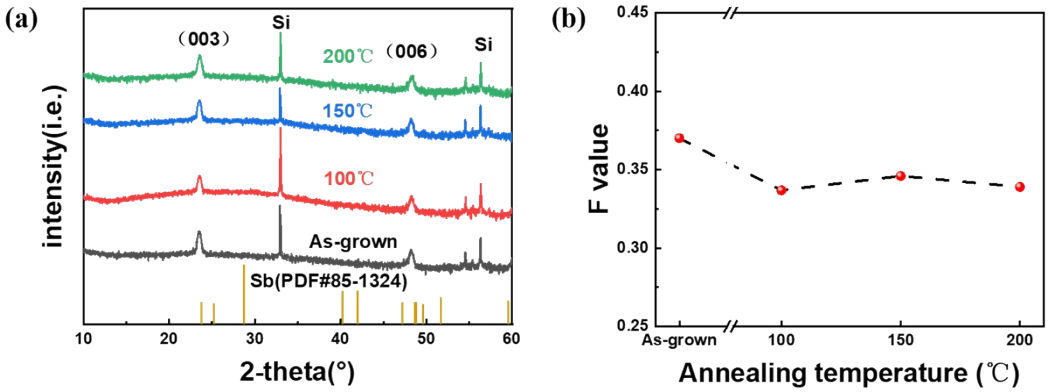

Figure S2 (a) XRD patterns and (b) F values of Bi_xSb_{1-x} annealed at different annealing temperatures

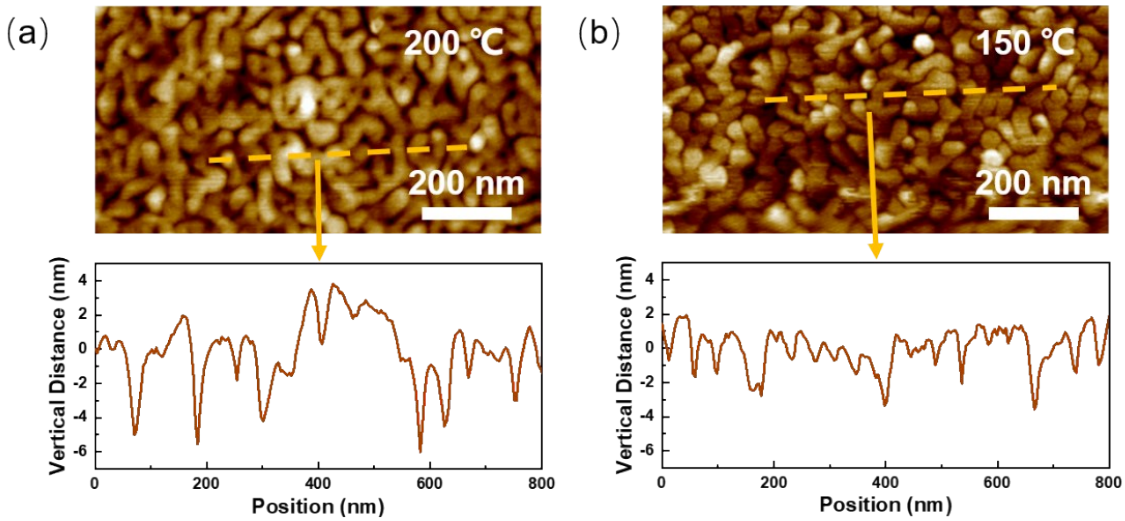

Figure S3 AFM images of Bi_xSb_{1-x} annealed at different temperatures (a) 200 ℃ and (b) 150 ℃

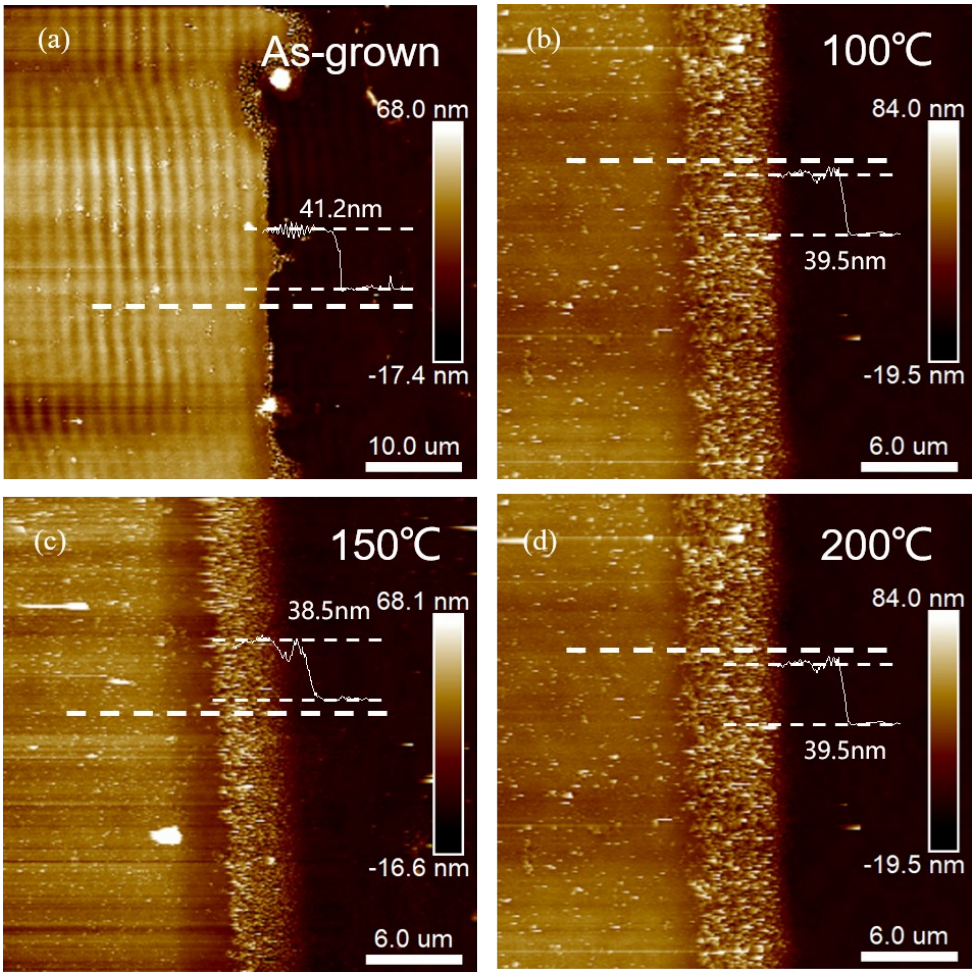

Figure S4 AFM images of the thickness of $(Bi_xSb_{1-x})_2Te_3$ processed at different annealing temperatures

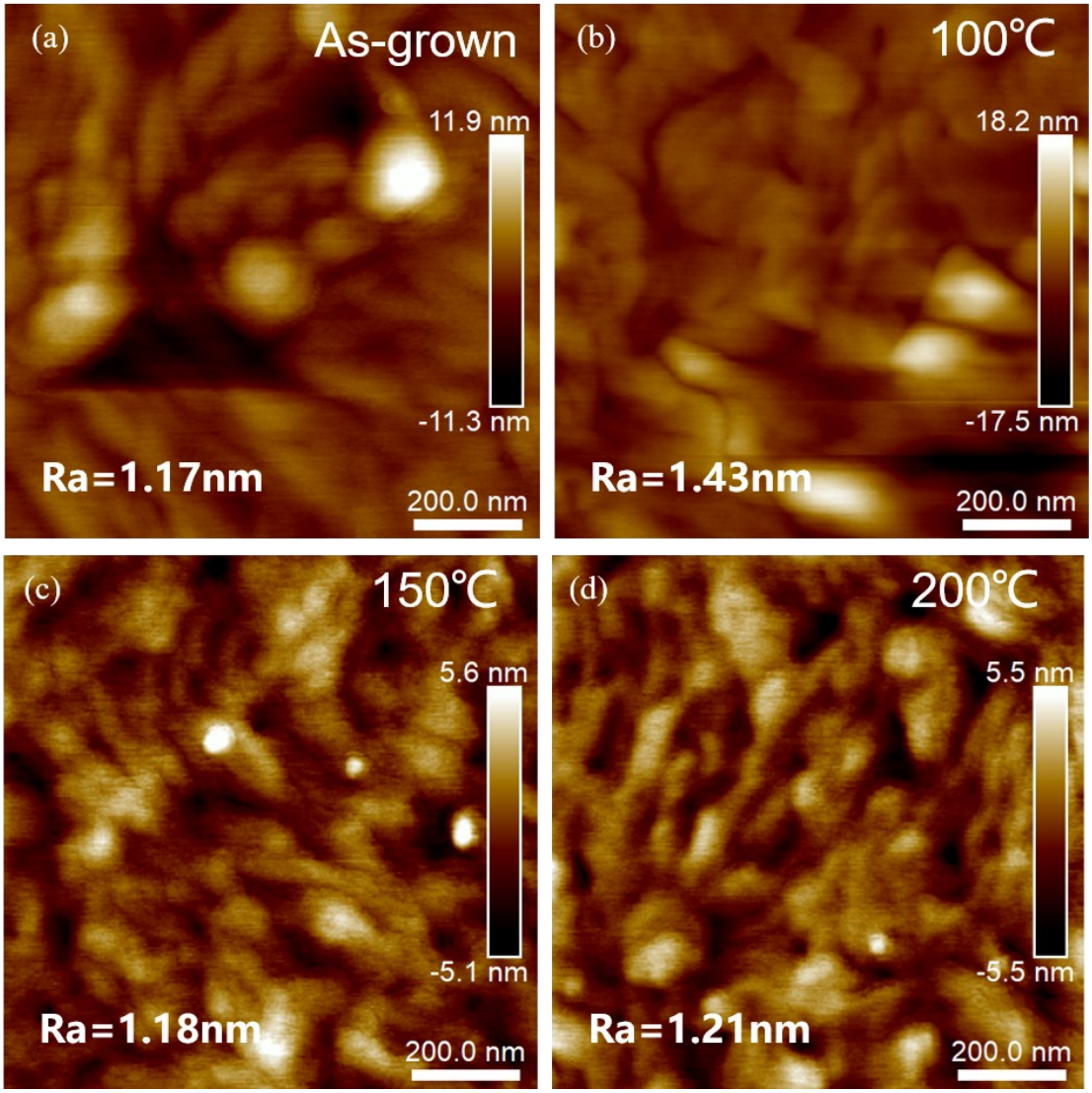

Figure S5 AFM images of the roughness of $(Bi_xSb_{1-x})_2Te_3$ processed at different annealing temperatures

Table S2 FWHM and crystalline size of $(Bi_xSb_{1-x})_2Te_3$ processed at different annealing temperatures

Annealing temperature	(006)		(0015)		Average size (nm)
	FWHM (°)	Crystalline size (nm)	FWHM (°)	Crystalline size (nm)	
As-grown	0.219	41.2	0.289	31.7	36.5
100°C	0.209	43.7	0.286	32	37.9
150°C	0.241	36.6	0.298	30.6	33.6
200°C	0.227	39.4	0.335	25.2	32.3

Table S3 Atomic composition of Bi_xSb_{1-x} annealed at different temperatures

Temperature	Bi (at.%)	Sb (at.%)
As-grown	2.36	97.64
100℃	1.74	98.26
150℃	2.99	97.01
200℃	0.36	99.64

Table S4 The room temperature electrical transport properties of $(Bi_xSb_{1-x})_2Te_3$ processed at different annealing temperatures

Annealing temperature	S (μV K^{-1})	n_H 10^{19}(cm^{-3})	μ (cm^2 V^{-1} s^{-1})	m_d^* (m_0)	E_F (meV)
As-grown	124.6	4.26	249.4	0.857	42.4
100℃	141.2	3.77	254.1	0.943	31.3
150℃	148.5	3.05	259.6	0.881	27.0
200℃	151.5	5.43	154.3	1.303	25.5

The density of states effective mass (m_d^*) is obtained from the Pisaranko plot in Figure 5(c) based on the SPB model. The equations are in the following:

$$S(\eta) = \frac{k_B}{e} \cdot \left[\frac{\left(\lambda + \frac{5}{2}\right) \cdot F_{\lambda+\frac{3}{2}}(\eta)}{\left(\lambda + \frac{3}{2}\right) \cdot F_{\lambda+\frac{1}{2}}(\eta)} - \eta \right] \#(1)$$

$$n_H = \frac{1}{e \cdot R_H} = \frac{(2m_d^* \cdot k_B T)^{\frac{3}{2}}}{3\pi^2\hbar^3} \cdot \left[\frac{\left(\lambda + \frac{3}{2}\right)^2 \cdot F^{\,2}_{\lambda+\frac{1}{2}}(\eta)}{\left(2\lambda + \frac{3}{2}\right) \cdot F_{\lambda+\frac{1}{2}}(\eta)} \right] \#(2)$$

$$F_i(\eta) = \int_0^\infty \frac{x^i}{1 + e^{x-\eta}} dx \#(3)$$

Where η is the reduced Fermi level, k_B is the Boltzmann constant, e is the electron charge, λ is the carrier scattering factor (λ = -1/2 for acoustic phonon scattering), R_H is the Hall coefficient, m_d^* is the effective mass, ħ is the reduced Plank constant, $F_i(\eta)$ is the Fermi integral.

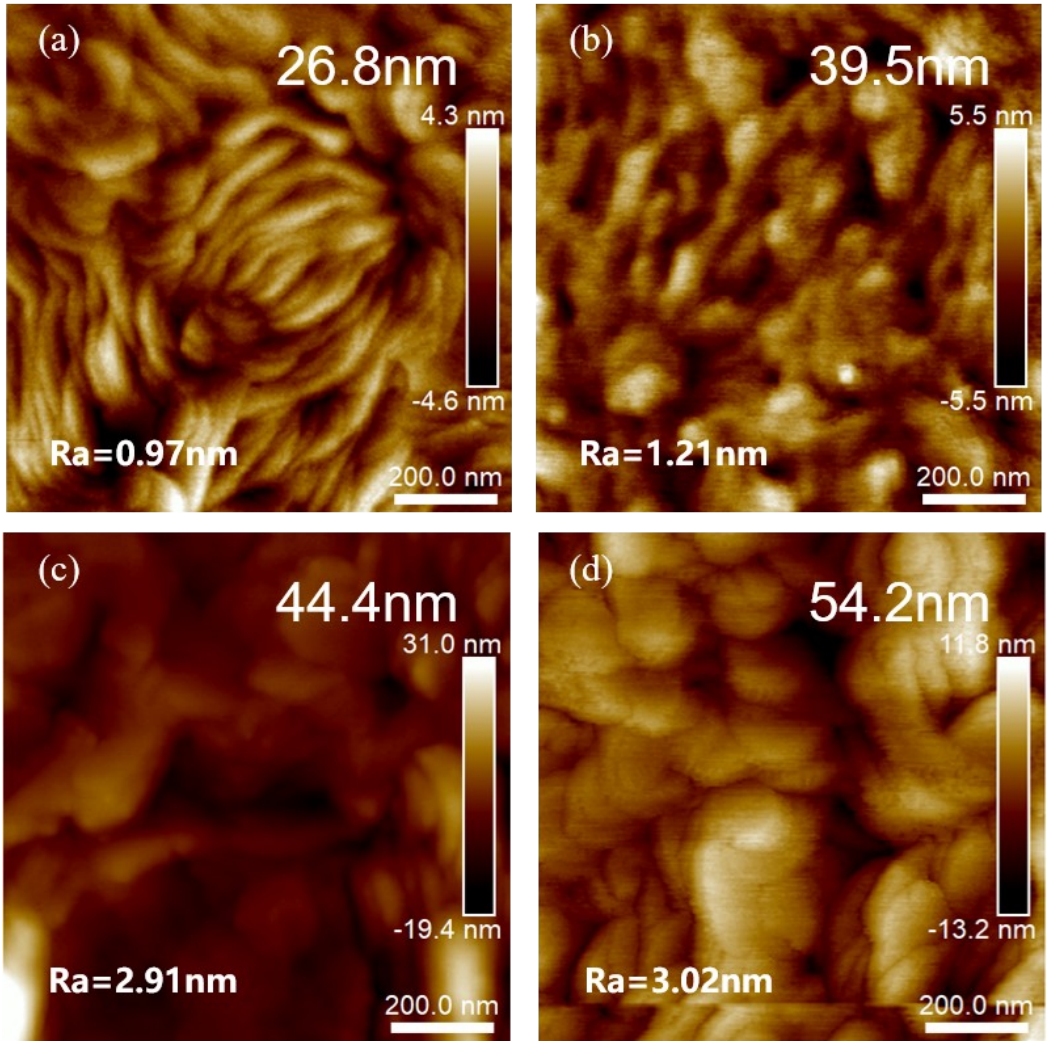

Figure S6 AFM images of the thickness of $(Bi_xSb_{1-x})_2Te_3$ with different thickness

Table S5 FWHM and crystalline size of $(Bi_xSb_{1-x})_2Te_3$ with different thickness

Thickness	(0 0 6)		(0 0 15)		Average size (nm)
	FWHM (°)	Crystalline size (nm)	FWHM (°)	Crystalline size (nm)	
26.8nm	0.291	29.4	0.384	23.2	26.3
39.5nm	0.227	39.4	0.335	25.2	32.3
44.4nm	0.211	43.4	0.298	30.6	37.0
54.2nm	0.155	68.0	0.238	39.8	53.9

Table S6 The room temperature electrical transport properties of $(Bi_xSb_{1-x})_2Te_3$ with different thickness

Thickness	S ($\mu V\ K^{-1}$)	$n_H\ 10^{19}(cm^{-3})$	$\mu\ (cm^2\ V^{-1}\ s^{-1})$	$m_d^*\ (m_0)$	E_F (meV)
26.8nm	116.3	4.10	131.4	0.763	48.6
39.5nm	151.5	5.43	154.3	1.303	26.6

44.4nm	150.4	4.34	184.4	1.132	26.1
54.2nm	145.8	5.84	190.5	1.317	28.8

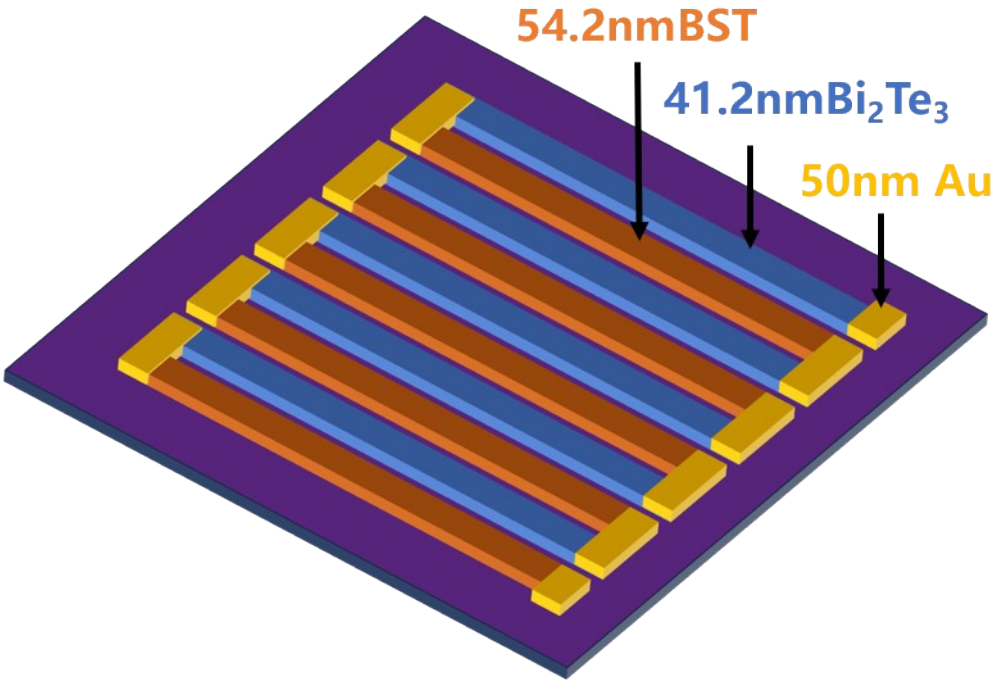

Figure S7 Schematic diagram of the structure of the thermoelectric device